Pergamon

Journal of Structural Geology, Vol. 18, Nos 2/3, pp. 295 to 309, 1996

0191-8141/96 $15.00 + 0.00

0191-8141(96)00111-5

Three-dimensional analyses of slip distributions on normal fault arrays with consequences for fault scaling

EMANUEL J. M. WILLEMSE, DAVID D. POLLARD and ATILLA AYDIN

The Rock Fracture Project, Department of Geological and Environmental Sciences, Stanford University, Stanford, CA 94305-2115, U.S.A.

(*Received* 4 *January* 1995; *accepted in revised form* 29 *August* 1995)

Abstract—Many fault arrays consist of echelon segments. Field data on ancient and active faults indicate that such segmented geometries have a pronounced effect on the distribution of fault slip. Outcrop measurements of slip on arrays of fault segments show that: (i) the point of maximum fault slip generally is not located at the centre of a fault segment; (ii) displacement gradients steepen towards the adjacent fault for underlapping faults; and (iii) displacement gradients become more gentle near the tips of overlapping faults.

Numerical analyses suggest that mechanical interaction between neighbouring faults may cause such asymmetrical slip distributions. This interaction occurs through local perturbation of the stress field, and does not require the faults to be connected. For normal faults, the degree of fault interaction, and hence the degree of asymmetry in the slip distribution, increases with increasing fault height and fault overlap and with decreasing fault spacing. The slip magnitude along a discontinuous fault array can be nearly equal to that of a single larger continuous fault provided the segments overlap with small spacing.

Fault interaction increases the ratio between fault slip and fault length, especially for closely spaced, overlapping faults. Slip-to-length ratios also depend on the three-dimensional fault shape. For normal faults, the slip-to-length ratio increases with increasing fault height. The effects of fault interaction and three-dimensional fault shape together can lead to more than one order of magnitude variation in slip-to-length ratio for the simple case of a single slip event in a homogeneous isotropic rock. One should expect greater variation for the more complex conditions found in nature. Two-dimensional fault scaling models can not represent this behaviour.

INTRODUCTION

Outcrop traces of many active and ancient faults are discontinuous, consisting of arrays of distinct segments (Tchalenko 1970, Tchalenko & Ambraseys 1970, Wallace 1973, Moore 1979, Segall & Pollard 1980, Barr 1985, Rippon 1985, Bouvier *et al.* 1989, Kronberg 1991). Figure 1 shows some examples of discontinuous normal faults at various scales. Small-scale, overlapping fault segments in the Jurassic Entrada sandstone (Arches National Park, Utah) are a few metres long and accommodate up to 150 mm of displacement (Fig. 1a). In the Volcanic Tableland (California), faults cutting through the Quaternary Bishop Tuff consist of segments that are tens of metres to several kilometres long and accommodate displacements of up to 100 m (Fig. 1b). The Bishop Tuff has been subjected to Basin and Range extension (Bateman 1965, Sherridan 1975). The 370 km long surface trace of the Wasatch fault zone (Utah) provides a large-scale example. Individual segments can be tens of kilometres long (Fig. 1c). Although it has not ruptured historically, palaeoseismological studies suggest several large-magnitude ruptures in Holocene times that delineate at least eight distinct rupture segments (Schwartz & Coppersmith 1984, Yeats & Schwartz 1990).

Such discontinuous or segmented faults are not only observed in map view, but also in cross-section (Aydin & Nur 1985). Discontinuities occur along dip-slip and strike-slip faults, both at the Earth's surface and in the subsurface, and at length scales that vary between millimetres and kilometres (Gay & Ortlepp 1979, Segall & Pollard 1980, Aydin & Nur 1982, Mandl 1987a,b, 1988, Larsen 1988, Gibbs 1990, Davy 1993). Discontinuous fault geometries are also reproduced in laboratory experiments (Cloos 1928, 1955, Riedel 1929, Gamond 1983, Naylor *et al.* 1986, Raynaud 1987, Filbrandt *et al.* 1994) and appear to be a fundamental property of faults. Outcrop traces for other faults may be continuous, but exhibit one or more jogs (see Fig. 1d for the terminology used in this paper). Such jogs may represent breached relays between originally discontinuous segments (Peacock & Sanderson 1994).

The discontinuous nature of faults has important consequences. The geometric irregularities near steps between individual fault segments play an important role in the initiation and termination of earthquake ruptures and in the distribution of aftershocks (Aki 1979, 1989, Bakun *et al.* 1980, 1986, Segall & Pollard 1980, King & Nabelek 1985, King 1986, Sibson 1986, 1987, 1989, Barka & Kadinshy-Cade 1988, King *et al.* 1990, Zhang *et al.* 1991). Palaeoseismological studies suggest that this behaviour is maintained during at least several earthquake cycles (Sieh 1981, Schwartz & Coppersmith 1984, Yeats & Schwartz 1990).

Fault segmentation also is important in a hydrogeological and petroleum geological context where fluid pathways may exploit relay zones between segments. Therefore segmented faults may not have a great fault-sealing potential, even if the fault gouge itself is fully sealing (Morley *et al.* 1990, Peacock & Sanderson 1994). Furthermore the complex slip variations observed along

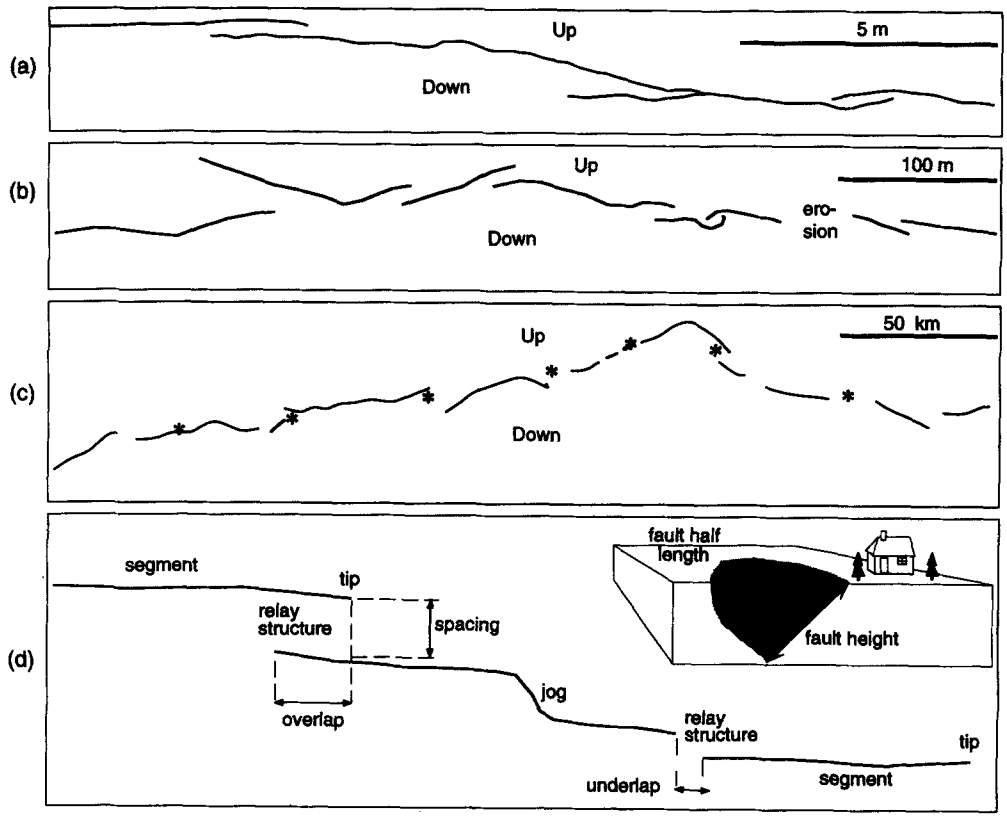

Fig. 1. Map traces of normal fault arrays at various scales. (a) Overlapping minor normal faults with both right and left steps in the Moab Member of the Jurassic Entrada Sandstone, Arches National Park, Utah. (b) A normal fault zone in the Bishop Tuff, Volcanic Tableland, California. Most fault segments overlap but appear to be discontinuous. (c) Wasatch fault zone, Utah. The discontinuous fault zone consists of underlapping and overlapping fault traces. Stars denote segment terminations inferred from palaeoseismological studies (Yeats & Schwartz 1990). (d) Terminology for the trace geometry of discontinuous fault zones. A *relay structure* is the zone connecting the footwall and hangingwall of a fault zone, where slip is transferred between segments (Goguel 1950, Larsen 1988). Reorientation of bedding at the fault step may create a *relay ramp* (Peacock & Sanderson 1991). Where segments link, the term *jog* has been used (Sibson 1986). Inset illustrates definitions of length and height of a fault surface (shaded).

segmented faults, especially near the relay structures between segments, complicate prediction of juxtaposition sealing in such areas and increase the risk of miscorrelating faults during seismic interpretation of the reservoir and aquifer structures.

The discontinuous nature of faults has important implications for conceptual models of fault generation and growth. According to one concept, a fault is a single smooth continuous surface of displacement discontinuity, which becomes larger as the slip across it increases (Watterson 1986, Walsh & Watterson 1987, 1988, Marrett & Allmendinger 1991, Cowie & Scholz 1992a,b,c). According to a second concept, faults grow primarily by the linkage of individual segments (Segall & Pollard 1980, Ellis & Dunlap 1988, Martel *et al.* 1988). Empirical and fracture mechanics models consistent with the first concept predict simple power-law relationships between fault length and slip: $D_{max} \sim L^c$, where D_{max} is the maximum slip and L the fault length. However, field data show considerable variability in slip-to-length ratios (Gillespie *et al.* 1992, Dawers *et al.* 1993, Scholz *et al.* 1993, Bürgmann *et al.* 1994). This variability appears, at least partly, to be related to fault growth by segment linkage (Peacock 1991, Peacock & Sanderson 1991), in agreement with sand-box experiments that reveal that slip-to-length ratios change significantly during the early stages of fault growth (Filbrandt *et al.* 1994). A second reason for scattered slip-to-length ratios is kinematic coherence (Walsh & Watterson 1991), and the difficulty of identifying the appropriate length for discontinuous faults. The distribution of total slip along an array of fault segments often resembles that of a single larger fault. The slip-to-length ratios of individual segments can be greater than the ratio for the composite fault zone (Dawers & Anders 1995).

Because of these practical consequences and theoretical implications, it is imperative to understand the mechanics of discontinuous faults. To date, most theoretical studies of ancient faults focus on one single fault and are based on two-dimensional models. For these models, the maximum slip is in the middle of the fault, and decreases according to some smooth function to zero at the fault tip-line (Walsh & Watterson 1988, Cowie & Scholz 1992b,c). In some cases, such relatively simple slip distributions are indeed observed (Muraoka & Kamata 1983, Rippon 1985, Barnett *et al.* 1987, Dawers *et al.* 1993). However, more complex and often asymmetrical slip distributions occur frequently, especially along segmented faults (Tchalenko & Berberian 1975, Deng *et al.* 1986, Rymer 1989, Peacock 1991, Peacock & Sanderson 1991, Dawers & Anders 1995).

In this paper we consider three-dimensional models of

normal faults or fault segments that interact mechanically with one another. After describing some natural examples of displacement variations along fault arrays, we use analytical solutions to the elastic boundary value problem to illustrate why three-dimensional analyses are necessary. Subsequently, we use three-dimensional numerical boundary element methods to investigate how slip may vary along two echelon fault segments. Then the analyses are expanded to arrays containing three or more segments. Comparisons between the three-dimensional model results and two-dimensional natural examples are used to document the strong relationships between three-dimensional fault shape, the spatial arrangement of individual segments within a fault zone, and the fault slip distributions. The consequences for fault slip-to-length ratios are also discussed.

SLIP VARIATIONS ALONG DISCONTINUOUS FAULTS

The displacement discontinuity or slip is one of the most fundamental physical quantities that can be used to characterize faults. Understanding the mechanics of faulting requires knowledge of the spatial and temporal variations in slip along neighbouring segments of discontinuous faults. The slip distributions can provide a quantitative assessment of the extent of mechanical interaction among the segments. For normal faults, scarp heights and offsets of layering or of seismic reflectors provide closely spaced measurements of slip distributions. These data facilitate the detection of subtle variations in slip and encourage quantitative analysis.

Field and laboratory observations

Slip variations along discontinuous earthquake surface ruptures have been measured by many investigators (Lawson *et al.* 1908, Tchalenko & Berberian 1975, Deng & Zhang 1984, Deng *et al.* 1986, Rymer 1989, Zhang *et al.* 1991). Detailed measurements along segmented ancient normal and strike-slip faults also are abundant (Walsh & Watterson 1990, Peacock 1991, Peacock & Sanderson 1991, 1994, Dawers & Anders 1995). Three-dimensional normal fault slip distributions that document the slip changes along the entire fault plane, rather than along a single section, are generated by combining slip measurements along a series of parallel cross-sections. Such three-dimensional slip distributions have been obtained from mine data (Rippon 1985), seismic data (Barnett *et al.* 1987, Bouvier *et al.* 1989, Jev *et al.* 1993, Childs *et al.* 1995) and sand-box experiments (Childs *et al.* 1993, Filbrandt *et al.* 1994).

Although the slip distribution over the surface of an isolated, single continuous fault may be relatively simple and approximately symmetrical (Fig. 2a), it is invariably less regular along the strike of segmented faults, especially near geometrical irregularities such as relay zones and jogs. Along each fault segment, slip varies from zero at both ends, to one or more maxima that generally occur somewhere in the middle third of the segment. Relays appear to be characterized by reduced fault slip. Variations in fault slip also are associated with regions where two normal faults overlap vertically (Rippon 1985).

The changes in fault slip near a relay zone appear to be systematic and to depend on spacing and the amount of fault overlap. A typical outcrop example (Fig. 2b) shows two *underlapping* normal faults mapped by Peacock & Sanderson (1991). The faults occur in Lower Jurassic limestones near Kilve, Somerset, U.K. (Peacock & Sanderson 1991). The underlapping faults show a steepening of the displacement gradient toward the relay. The second example (Fig. 2c) shows kilometre-scale *overlapping* normal faults in the Volcanic Tableland, California (Scholz *et al.* 1993, Dawers & Anders 1995). These fault segments, which are part of a longer fault array, also show steeper displacement gradients where the faults enter the relay ramp. However, closer to the fault tips in the relay zone, the gradient becomes more gentle. Both the underlapping and overlapping fault segments (Figs. 2b & c) show that the maximum slip is generally not located at the segment centre, but consistently occurs closer to the relay.

These two field examples illustrate features of slip distributions that are observed at the centimetre scale in sand-box experiments and at the kilometre scale in three-dimensional seismic surveys (Childs *et al.* 1993, 1995). The decrease in displacement gradient toward the fault tips of overlapping segments (Fig. 2c) is only detectable when the data points are closely spaced. Commonly, however, the fault slip data are relatively widely spaced, giving the false impression that displacement gradients remain steep throughout relays. The two styles of slip distribution shown in Figs. 2(b) & (c) may both occur along a particular normal fault array, depending on whether adjacent segments overlap or underlap. Similar observations can be made along strike-slip faults (Rymer 1989). Although we have illustrated systematic slip changes near relays using examples of ancient faults, that may have accumulated such slip over many earthquake cycles (Watterson 1986), the same features are also observed for single event slip distributions obtained after earthquakes on active faults (Sieh 1978, Deng & Zhang 1984, Rymer 1989, Thatcher & Bonilla 1989).

Existing models

Fracture mechanics models of a single fault subjected to a uniform remote shear stress and a lesser uniform shear traction on the fault surfaces predict an elliptical variation in slip for a single event (Pollard & Segall 1987). However, earthquake data show that many single slip events are characterized by slip distributions that taper more linearly towards the tips (Deng *et al.* 1986, Rymer 1989). Cowie & Scholz (1992a), building upon the 'cohesive end-zone' models by Palmer & Rice (1973) and Rice (1979), show that an increase in frictional

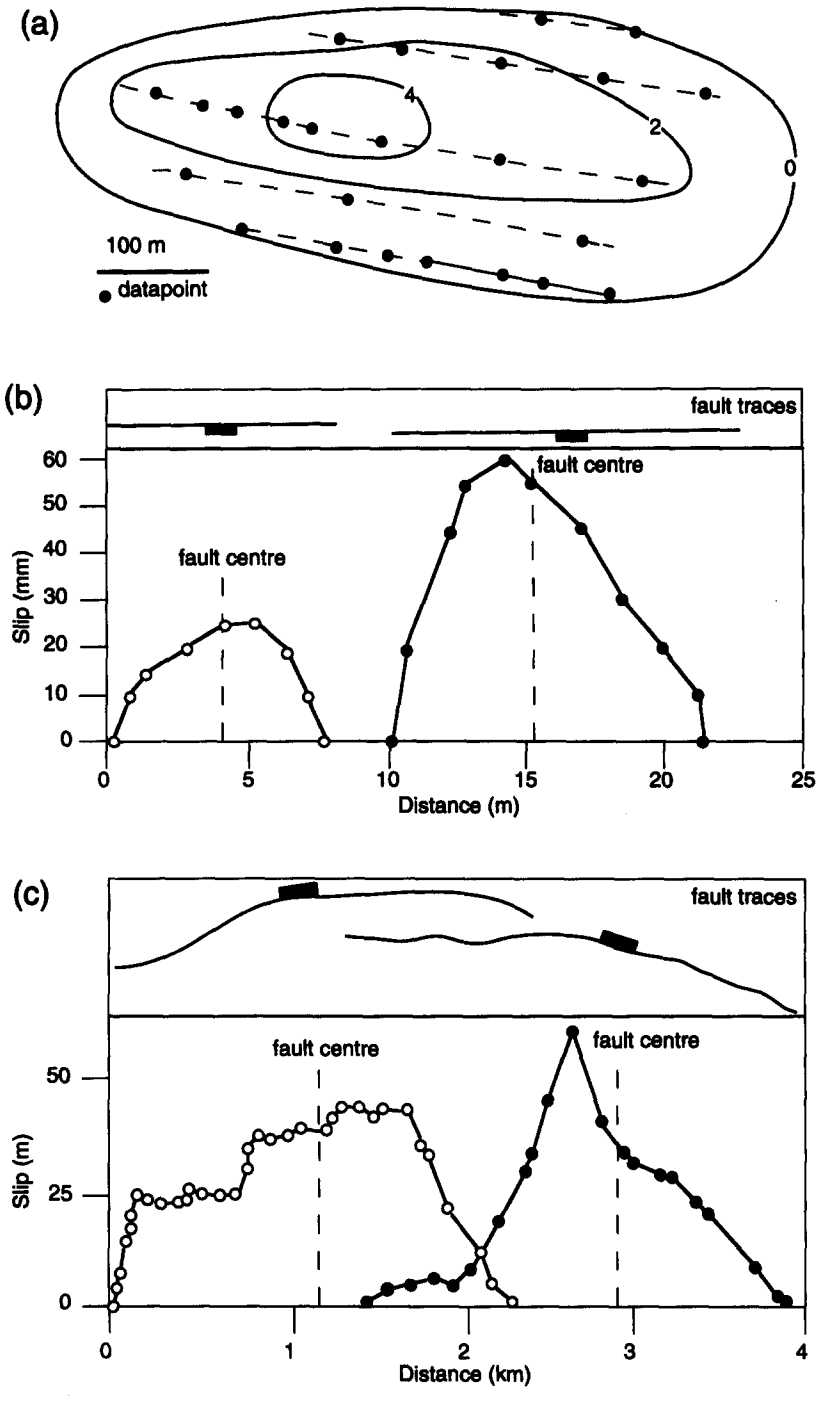

Fig. 2. Fault slip distributions along normal faults. (a) Contoured three-dimensional distribution of vertical component of slip along a single, continuous normal fault plane (after Rippon 1985). Contour values are in metres. The data are measurements of coal layer offset at several levels (indicated by dashed lines) of a mine in Derbyshire, U.K. (b) Minor underlapping faults exposed in Jurassic limestones near Kilve, Somerset, U.K. (Peacock & Sanderson 1991). Note the asymmetry in the slip distribution, the off-centre location of maximum slip, and the steep slip gradients near the inward fault tips. (c) Overlapping normal faults in the Quaternary Bishop Tuff, Volcanic Tableland, California. The slip distribution on each segment is asymmetrical. The maximum slip occurs off-centre, and the fault slip gradient is relatively steep where the fault enters the relay structure, and very gentle near the fault tips in the relay zone (after Scholz *et al.* 1993 and Dawers & Anders 1995).

resistance towards the fault tips can lead to tapered slip distributions for single events.

Watterson (1986) and Walsh & Watterson (1987, 1988) postulate that ancient faults may be the cumulative result of many slip events. They show how the sum of many elliptical slip distributions can result in a more linear cumulative slip distribution if each slip event involves fault propagation. Cowie & Scholz (1992a) postulate that the tapered shape of the slip distribution for cohesive end-zone faults does change when summing many slip events. Whereas Walsh & Watterson predict an increase in the fault slip-to-length ratio for each slip event, Cowie & Scholz predict a constant slip-to-length ratio. Both models, whether applied to active or ancient faults, predict simple symmetric slip variations. Some single, isolated faults indeed exhibit such slip distri-

butions (Muraoka & Kamata 1983, Rippon 1985, Barnett *et al.* 1987, Cowie & Scholz 1992c). However, the complex, asymmetrical slip distributions along segmented faults can not be addressed with these models and thus require further analysis.

Two-dimensional analyses have shown that mechanical interaction between fault segments strongly influences the slip along strike-slip fault arrays (Segall & Pollard 1980, Martel & Pollard 1989, Aydin & Schultz 1990, Bürgmann *et al.* 1994) and the amount of opening along dyke arrays (Delaney & Pollard 1981). Relative movement across one segment leads to a local perturbation in the stress field. This perturbation influences the traction and hence the relative movement on neighbouring segments. The increase in shear stress ahead of a fault tends to locally enhance the movement on neighbouring faults in that region. Conversely, the decrease in shear stresses to the side of a fault (the 'stress shadow') tends to locally reduce slip on neighbouring faults there. Although very detailed slip distributions are available for normal fault arrays, the effect of mechanical interaction among the segments has not been investigated to date.

SLIP ALONG AN ISOLATED SINGLE NORMAL FAULT

Natural faults are not infinite in one direction and do not have the blade-like shape postulated in two-dimensional models. Three-dimensional fault shape influences the magnitude of fault slip, and controls the magnitude and spatial distribution of stress enhancement or stress reduction that drives mechanical fault interaction. Both points can be illustrated using the analytical solution for a single elliptical crack subject to a uniform stress drop and embedded in a homogeneous, isotropic, linearly-elastic medium (Sih 1975, Tada *et al.* 1985). According to this solution, which forms a simple model for a single slip event, the maximum amount of slip across a fault depends on the elastic shear modulus, Poisson's ratio, and on the fault aspect ratio. The fault aspect ratio is defined here as the fault length (measured as the trace length on a horizontal plane going through the centre of the fault) divided by the fault height (measured along the fault surface in the dip direction, see Fig. 1d).

We have used the analytical solution to calculate the maximum fault slip as a function of fault aspect ratio for various values of Poisson's ratio (ν). For all cases shown in Fig. 3, the normal faults have the same horizontal length. This is meant to represent the typical situation encountered in the field, where one can reliably measure the horizontal fault trace length, without knowing the fault dimensions in the dip direction. The maximum fault slip decreases as the fault height decreases (i.e. increasing aspect ratio). The two-dimensional, pure mode III crack solution is also shown, representing the limiting case of an 'upright' ellipse with zero aspect ratio. The effect of Poisson's ratio is minor, with perfectly compressible rocks ($\nu = 0$) accommodating somewhat larger slips than nearly incompressible rocks ($\nu = 0.49$).

The magnitudes of the stress components around the fault are directly proportional to the slip magnitude. The size of the region of perturbed stress scales with the size of the fault surface. The three-dimensional spatial distribution of the stress perturbation is quite complex. Figure 4 illustrates the stress perturbation around a single isolated, vertical circular normal fault subjected to a complete stress drop. This stress distribution can be calculated by solving the appropriate equations in Sih (1975). Shaded areas mark local increases in shear stress acting on planes parallel to the fault and in the direction of the fault slip vector, with the remaining areas (unshaded) being characterized by a shear stress reduction. A vertical cross-section through the centre of this circular fault model (Fig. 4a) reveals a stress perturbation that is similar, but not identical, to that around a two-dimensional mode II crack (Segall & Pollard 1980). A horizontal cut through the centre of the fault, providing the equivalent of a map view (Fig. 4b), shows that the stress perturbation is somewhat like that of a two-dimensional mode III crack (Sih 1975, Tada *et al.* 1985).

The spatial distribution of the stress perturbation is complex due to both the finite size of the slipping surface and the continuously changing angle between the fault slip vector and the tip-line orientation. To compare different fault shapes, consider the fault length constant. For lesser fault aspect ratios (i.e. taller faults), the stress perturbation extends farther from the fault, affecting a larger volume. For greater fault aspect ratios (i.e. vertically short faults), the stress perturbation is limited to the immediate fault vicinity.

MECHANICAL INTERACTION AND SLIP ALONG SEGMENTED NORMAL FAULTS

Available three-dimensional analytical techniques are limited to the analysis of a single fault of simple geometry such as penny-shaped or elliptical (Eshelby 1957, Rudnicki 1977, Rice & Rudnicki 1979, Rudnicki 1979, Tada *et al.* 1985). The mechanical interaction between several faults can only be investigated numerically. We have used Poly3d, a three-dimensional boundary element program based on the displacement discontinuity method (Thomas 1993). A detailed treatment of boundary element techniques in solid mechanics is given by Crouch & Starfield (1983) and Becker (1992). The boundary element procedure has the advantage that only the faults themselves need to be meshed, using a set of elements with prescribed displacement discontinuities or tractions. The fundamental solution used by Poly3d is that of an angular dislocation in a linear-elastic half-space (Comninou & Dunders 1975, Jeyakumaran *et al.* 1992). The boundary of the half-space represents the traction-free surface of the Earth. Several angular dislocations are combined to form a planar polygonal element of constant displacement discontinuity or slip. By joining many polygonal elements, one or more faults

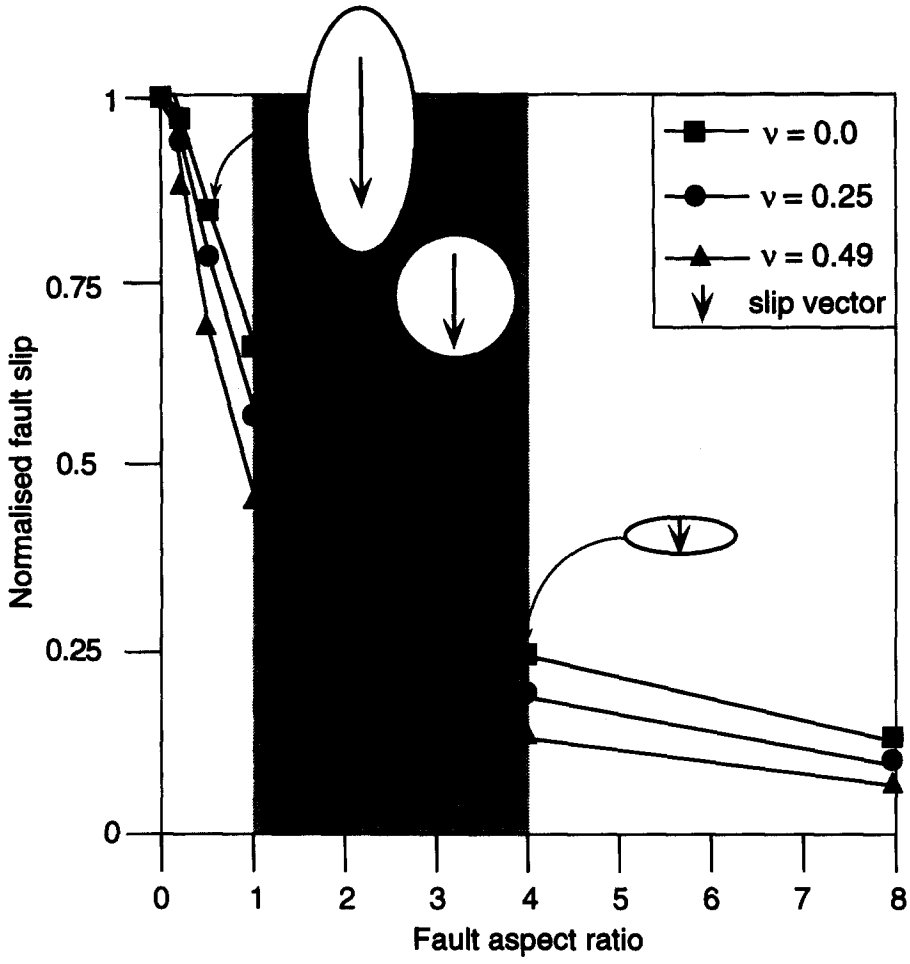

Fig. 3. Effect of fault aspect ratio and Poisson's ratio on maximum fault slip. The maximum fault slip is divided by the maximum slip that occurs along a two-dimensional pure mode III crack. For all cases, the horizontal fault length is constant. Vertically tall faults (greater aspect ratio) have a greater maximum slip than short faults (lesser aspect ratio). Changes in fault shape have a larger effect than variations in Poisson's ratio. All fault models postulate a complete, uniform shear stress drop.

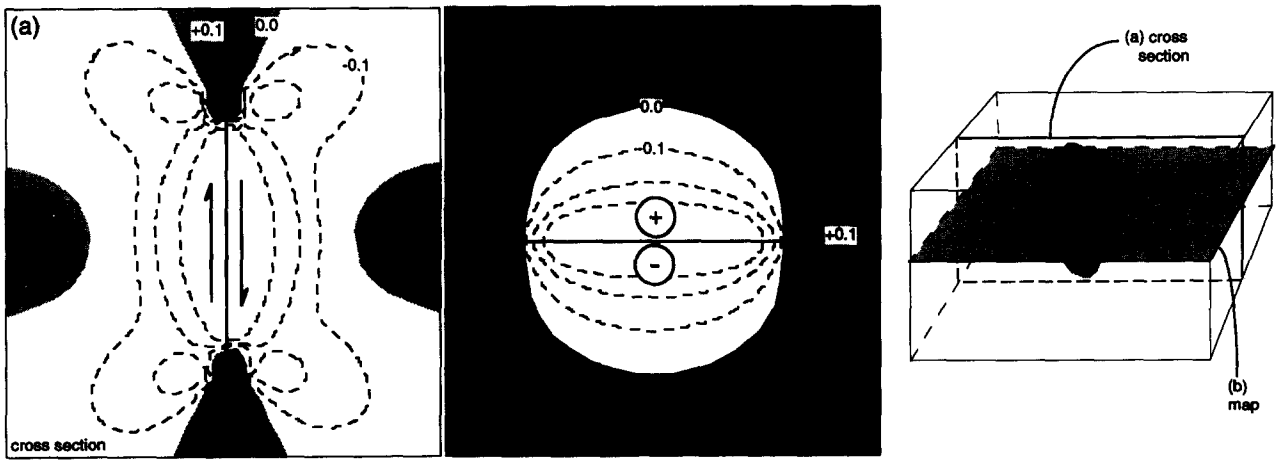

Fig. 4. Contoured distribution of fault-parallel shear stress, acting in the direction of the fault slip vector, about a vertical circular normal fault with a complete and uniform stress drop: (a) vertical cut through the three-dimensional model provides a cross-section view in which the stress perturbation is similar, but not identical, to that about a two-dimensional pure mode II crack; (b) horizontal cut through the three-dimensional model provides a map view, in which the stress perturbation is somewhat like that about a two-dimensional pure mode III crack. The shear stress is enhanced in the shaded areas, and is reduced in the unshaded areas. Parts of a hypothetical neighbouring parallel fault situated in the shaded areas would locally experience enhanced slip whilst the slip would locally be reduced if this neighbour were located in the unshaded areas.

with varying slip can be modelled (Fig. 5a). Because the displacement discontinuity is constant across each element, slip varies over the entire fault surface according to a set of step functions. By using many small elements, smooth fault slip distributions can be approximated. The faults need not be planar and can have irregular tip-lines.

By prescribing traction boundary conditions at the centre of each polygonal element, mechanical interaction between faults can be modelled. This is done by solving a series of linear algebraic equations that describe the influence of each element on all other elements (Crouch & Starfield 1983, Becker 1992). Poly3d therefore offers some advantages over the approach by Ma & Kusznir (1993), which allows multiple faults only by simple superposition, thus neglecting mechanical interaction. Poly3d also can compute the stress, strain and displacement fields in the material surrounding the fault(s), but it can not model actual fault propagation or stress relaxation during accumulation of slip in a series of events.

In the first suite of numerical experiments, the faults are loaded remotely by a unit shear stress, and the fault surfaces themselves are free of shear traction (Fig. 5b). The uniform drop in shear stress leads to an elliptical variation in slip for the case of an isolated fault. The displacement discontinuity perpendicular to the fault was prescribed to be zero, thereby preventing opening or interpenetration of the fault walls (Fig. 5b). These models only address fault interaction through perturbation in shear stress. Changes in frictional resistance due to increase or decrease of normal stress at contractional or extensional relay zones are not taken into account. These boundary conditions should be considered a first approximation that will nonetheless capture some of the principal effects of mechanical interaction. For example, two-dimensional analyses by Aydin & Schultz (1990) that incorporated a Coulomb friction criterion on the faults suggest similar behaviour for faults with and without friction.

Mechanical interaction between two circular faults

The model consists of two circular normal faults that dip 60° and are not linked (Fib. 5b). In order to minimize additional complexities due to proximity to the traction-free surface of the Earth, the faults are embedded in an elastic whole-space. This corresponds to faults being buried deeper than about 10 times their diameter. The centres of both faults are at the same depth (Fig. 5b). The elastic medium is characterized by a Poisson's ratio of 0.25 and a unit shear modulus. The effects of lateral fault overlap have been analysed using a number of different model geometries. The fault overlap is defined as the horizontal distance between the fault tips measured in the strike direction on a horizontal plane through the fault centres (Figs. 1d and 5b). In the simulations, the overlap varies between $+0.5a$ and $-0.5a$, where a is the fault radius and negative values indicate fault underlap. The fault spacing is defined as the horizontal distance between the fault surfaces measured perpendicular to their strike in a horizontal plane through their centres (Figs. 1d and 5b). The spacings considered here range between $0.1a$ and $0.05a$.

Figure 6 summarizes the results for two faults spaced at $0.05a$, showing contours of elevation changes across a horizontal 'observation' plane through the fault centres (Fig. 6a) and contours of the computed slip on the left fault (Fig. 6b), and the slip distribution along a horizontal line through the centre of the left fault (Fig. 6c). Slip on the right fault is simply the mirror image of that on the left fault. The contour maps in Fig. 6(a) show footwall uplift (solid contours) and hangingwall subsidence (dashed contours). The fault slip in Figs. 6(b) & (c) is normalized to the maximum slip that would occur on an isolated fault. For a large underlap (left-hand drawings)

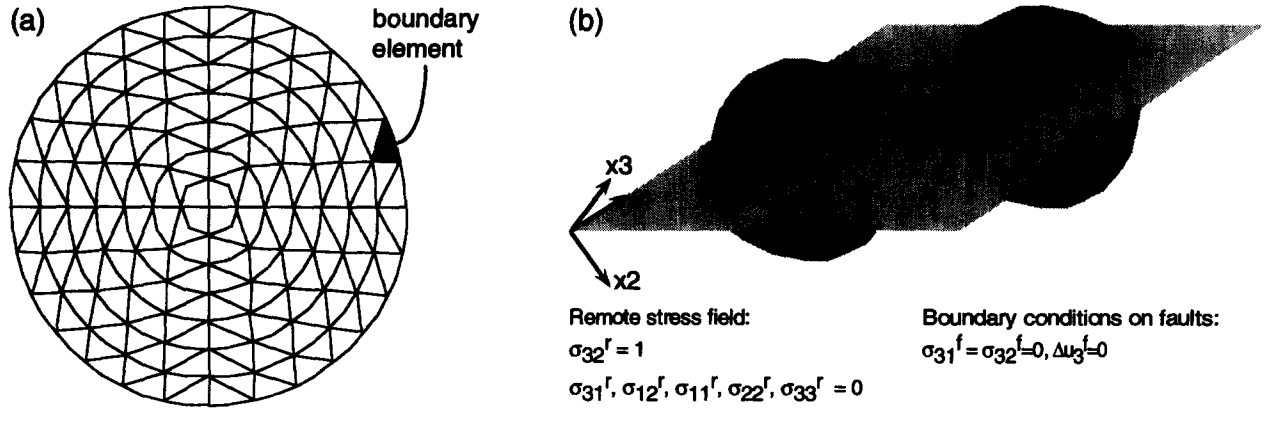

Fig. 5. Model geometry and boundary conditions. (a) Typical mesh used to model a fault, consisting of concentric rings of quadrilateral elements. The quadrilateral nature of the elements is visible only near the fault centre. (b) Model geometry, consisting of two deeply buried circular normal faults with their centres at the same depth. The faults dip 60°. A horizontal 'observation' plane through fault centres is used to analyse footwall uplift and hangingwall subsidence. Remote and fault boundary conditions represent a complete uniform shear stress drop ($\sigma_{32}^r - \sigma_{32}^f = 1$). The fault walls are not allowed to come apart or interpenetrate ($\Delta u_3^f = 0$). σ indicates stresses–tractions, Δu indicates displacement discontinuity, and the subscripts r and f refer to values in the remote field and on the faults, respectively. The x_1-direction is parallel to fault strike, the x_2-direction is parallel to fault dip direction and the x_3-direction is normal to fault plane.

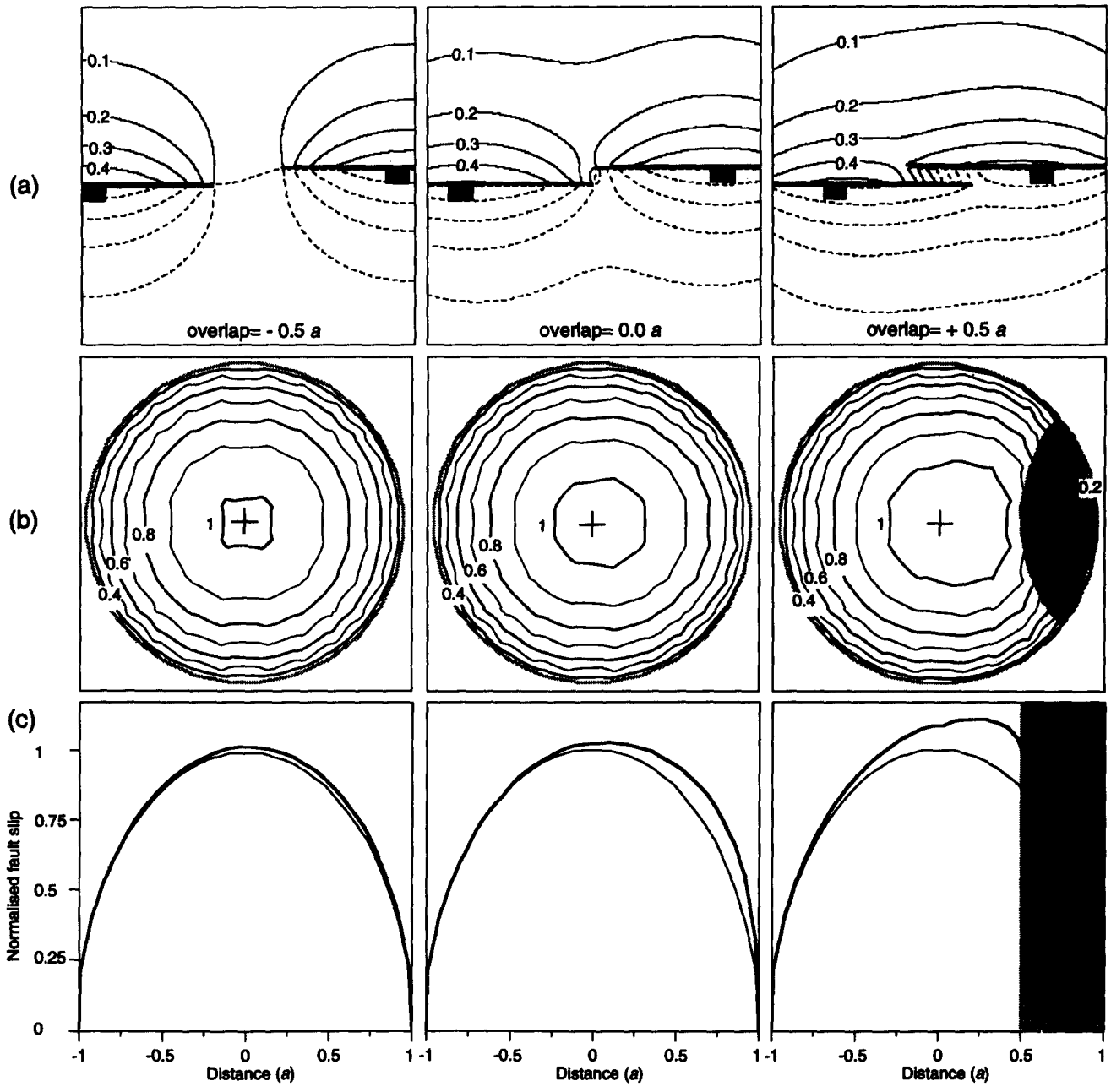

Fig. 6. Slip and wall rock deformation for two circular echelon normal faults for various degrees of fault overlap. The fault spacing is $0.05a$, where a is the fault radius. (a) Contours of vertical displacement on a horizontal plane through the centres of the faults. Solid contours indicate uplift above datum level and dashed contours indicate subsidence below the datum level. The contours delineate two separate structures for the case of underlapping faults (left), but a single, larger structure for the case of overlapping faults (right). Also note the asymmetrical footwall uplift and hangingwall subsidence immediately adjacent to the overlapping faults (right). Solid bar indicates down-thrown side of fault, and marks the position of fault centres. (b) Contours of slip on the left fault. A contour value of 1 indicates the maximum slip that would occur on a single isolated fault. For significantly underlapping faults (left), the contours remain nearly perfectly symmetrical and closely resemble the elliptical slip distribution of an isolated fault. With increasing fault overlap, the magnitude of the maximum slip increases, and is located further off-centre. The slip distribution differs considerably from that on a single isolated fault. Cross indicates fault centre and shading in the right-hand diagram outlines the area of overlap with the neighbouring fault. (c) Slip distribution on left fault along a horizontal line through its centre. Thick black curves show computed slip distribution and thin black curves represent slip along a single isolated fault. The differences between both curves are caused by mechanical interaction.

the faults do not interact significantly: the slip distribution on the faults follows a nearly elliptical pattern and the maximum slip occurs near the fault centre (Figs. 6b & c). Comparison of the underlapping fault geometry with the stress perturbation shown in Fig. 4(b) shows that each fault is subjected to a moderately increased shear stress caused by movement on its neighbour. The moderate increase in shear stress leads to a slip magnitude that is slightly greater than that on an isolated fault (for which the maximum normalized slip is 1).

For zero fault overlap (Fig. 6, middle diagrams), the maximum slip increases significantly, and is located off-centre towards the relay zone. Also, the outermost slip contour is deflected towards the relay zone (Fig. 6b).

These observations indicate that the displacement gradient is steeper on the right-hand (relay) side than on the left-hand (distal) side of the fault. This result can be understood by comparing the fault arrangement with the stress perturbation shown in Fig. 4(b). Because the faults have zero overlap, movement on each fault causes a significant increase in driving stress on the neighbour, especially in the relay area. The resulting asymmetrical distribution in shear stress causes the off-centre location of maximum slip and the changes in displacement gradient discussed above. The computed asymmetrical shape of the slip distribution correlates well with the natural example shown in Fig. 2(b) and with three-dimensional slip distributions along buried underlapping faults (Childs *et al.* 1995).

For overlapping faults (Fig. 6, right-hand diagrams), the magnitude of the maximum slip is greater than in the two earlier cases (about 1.09 times the slip on an isolated fault), and occurs at a larger distance from the fault centre. For the left fault, the area of maximum slip moves towards the right, i.e. towards the relay zone. The slip gradient is therefore more gentle on the left-hand (distal) part of this fault (Fig. 6c). Similarly to the above cases, the *average* slip gradient is steeper on the right-hand (relay) side. However, the slip distribution on the relay side is more complex. In the area of fault overlap (shaded in Figs. 6b & c, right-hand diagrams), the contours of fault displacement depart significantly from the concentric circular pattern. The contours are deflected away from the relay zone becoming straighter and approximately equally spaced throughout the area of fault overlap, indicating a nearly linear change in fault slip. Relative to the elliptical slip distribution along isolated faults, the slip gradient near the tip has decreased significantly (Fig. 6c). However, farther from the fault tip-line, in the region between the relay zone and the point of maximum fault slip, the gradient is steeper compared to that on an isolated fault.

The complex slip distribution for overlapped faults can again be understood by comparing the fault geometry with the stress perturbation shown in Fig. 4(b). Movement on one fault causes a decrease in driving stress on the overlapping part of the neighbouring fault that is located in the relay area, but an increase along the remaining distal parts of the neighbour. These changes in driving stress correspond to a decrease and increase of slip respectively. Both the flattening and steepening of the slip distribution along the fault, and the off-centre location of maximum fault slip correlate well with the observations on natural faults (e.g. compare Fig. 2c and Fig. 6c). Therefore a reduction of slip gradient near the fault tip is not necessarily caused by a cohesive end-zone (Cowie & Scholz 1992c), but can also be caused by interaction with a neighbouring fault. Similar behaviour in the relay zone is seen on three-dimensional slip distributions for overlapping faults in sandbox experiments (e.g. fig. 11 in Childs *et al.* 1993).

The degree of fault interaction decreases with increasing segment spacing. The distance at which the interaction between faults becomes negligible depends on the three-dimensional fault shape. Vertically tall normal faults can interact across large distances because the stress perturbation extends farther from the fault. The extreme case consists of infinitely tall pure mode III faults. Even in that case, the effects of mechanical interaction and the deviations from the elliptical slip distribution are negligible if they are separated by more than their half lengths. Vertically short faults may not interact significantly even if they are closely spaced because the stress perturbation decays very rapidly with distance from the fault. In general, the region of influence scales with the shortest dimension of the fault.

The above three-dimensional results are in agreement with other studies. For example, two-dimensional models for strike-slip faults show that the stress intensity factor for the proximal (relay) fault tip is enhanced for underlapping faults, and decreases sharply for overlapping faults (Martel & Pollard 1989, Aydin & Schultz 1990). These changes in the magnitude of the near tip stress concentration are equivalent to an increased slip gradient near the proximal tips of underlapping faults and a decreased slip gradient at the proximal tips of overlapping faults. This is consistent with the results shown in Fig. 6, and suggests that segments with underlapped geometry will tend to grow, whereas segments with appreciable overlap will tend not to propagate. This might explain why underlapped geometries are rare and overlapped geometries are more common (Aydin & Schultz 1990), and also why faults generally overlap for limited distances relative to their spacing. The three-dimensional models shown here highlight how these effects of mechanical interaction change along the fault tip-line.

Arrays containing more than two faults

Figure 7 shows a model of three mechanically interacting faults with a spacing of $0.05a$ and an overlap of $0.5a$. The response is similar to that discussed above. Slip (thick black curve) on each outer fault segment increases the shear stress on the central part of the middle fault segment. Therefore the slip on the middle fault segment is enhanced by two neighbours on either side, resulting in an even greater maximum slip than in the case of two echelon faults (about 1.16 times that for an isolated fault: thin black curve). The mechanical effects of the outer segments on the central segment are symmetric, so that the maximum slip on the middle fault occurs at the centre. Because the central fault has the largest slip, its average slip gradient is greater than that of the neighbouring faults. The asymmetrical slip on the two outer segments is similar to the response of the two interacting faults because they experience an asymmetrical perturbation in shear stress that is mostly driven by the central segment.

These model results correlate well with field observations. Figure 8 shows slip distributions for two normal fault arrays, one from the Arley Coal Seam at Nook Colliery, Lancashire, U.K. (Walsh & Watterson 1990), and the other from the Bishop Tuff in the Volcanic

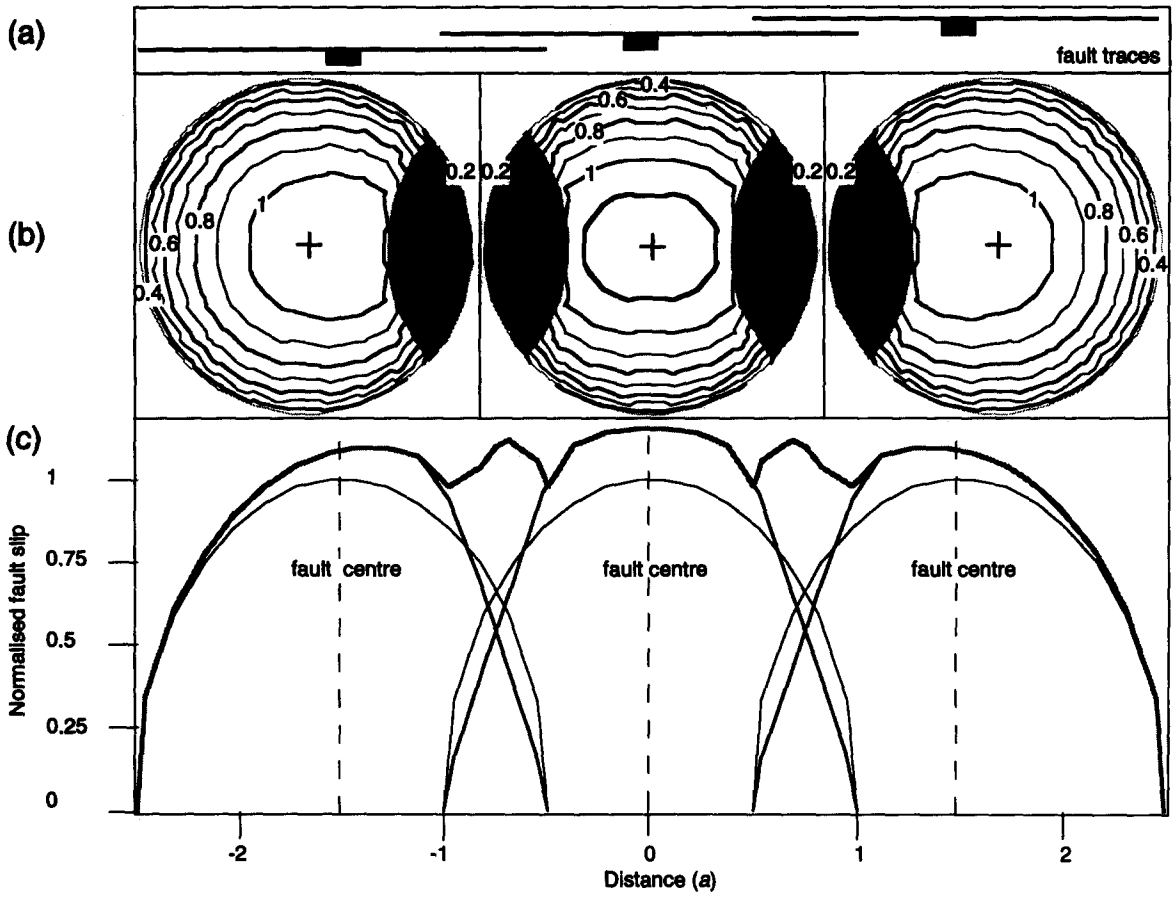

Fig. 7. Slip distribution for an array of three overlapping circular normal faults. (a) Fault trace geometry as observed on a horizontal plane through the fault centres. The fault overlap is $0.5a$, and the fault spacing $0.05a$. (b) Contours of normalized slip. Mechanical interaction leads to asymmetrical slip distributions on the two outer fault segments. Shaded areas indicate where faults overlap. (c) Slip distribution along a horizontal line through the centre of the three faults. Comparison between the modelled slip distribution (thick black curves) and the slip distribution without mechanical fault interaction (thin black curves) reveals the increase in maximum slip along each segment, and the asymmetry in slip distribution on the outer two segments. The total slip across the array (thick grey curve) has the appearance of one larger fault with slightly irregular slip distribution.

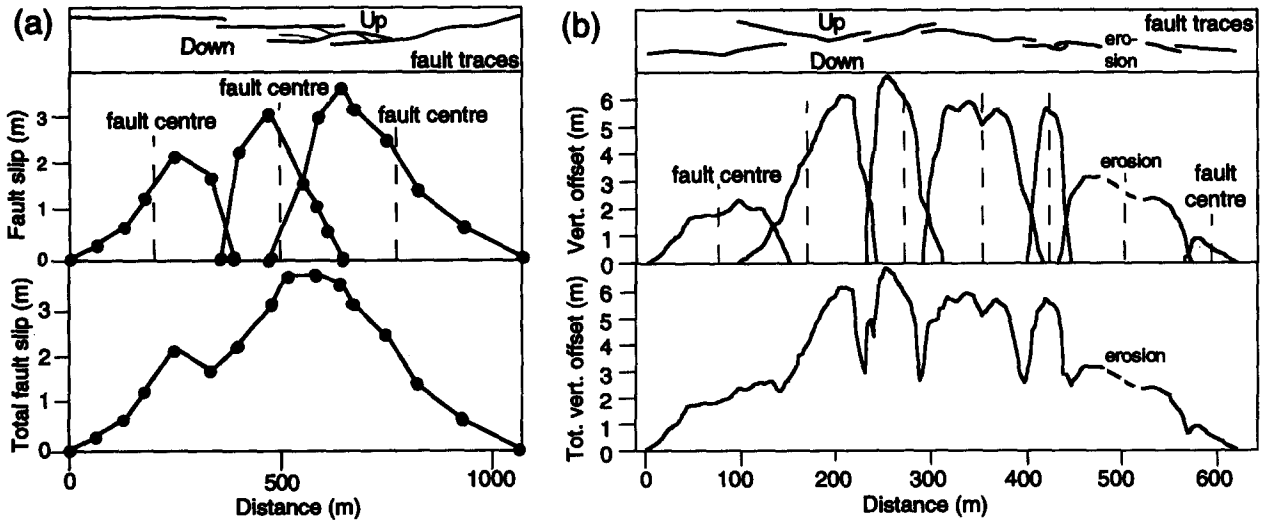

Fig. 8. Slip distributions along normal fault arrays indicating kinematic coherence. (a) Slip distribution along normal fault array in the Arley coal seam in Nook Colliery, U.K. (after Walsh & Watterson 1990). (b) Slip distribution along echelon normal fault array in the Bishop Tuff, Volcanic Tableland, California. Total slip across the entire array has the appearance of one larger fault. The slip minima are associated with the relay structures.

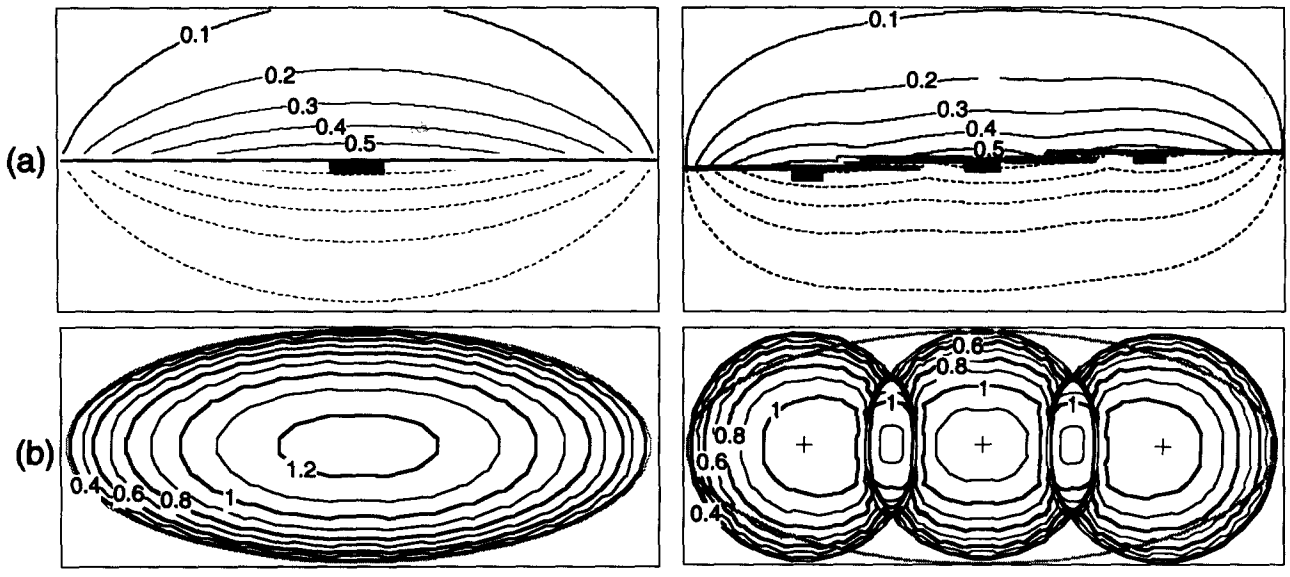

Fig. 9. Comparison between a single elliptical fault and a fault array of the same length. (a) Fault trace geometry and contours of vertical displacement on a horizontal plane through the centres of the fault(s). The single elliptical fault (left) has the same dimensions as the envelope surrounding the three echelon faults (right). Solid contours indicate uplift above datum level and dashed contours indicate subsidence below the datum level. (b) Contours of normalized slip. For the fault array, the contours delineate total slip accommodated across the array, which is obtained by summing the slip on the individual segments. The grey ellipse on the right shows the tip-line shape of the elliptical fault shown on the left.

Tableland, California. The slip on the latter array was obtained by surveying the fault scarps in a manner similar to that described by Dawers *et al.* (1993). Despite the irregularities in fault geometry for these natural examples, the predicted relative effects of fault interaction are clearly recognizable in the field data: (i) off-centre location of maximum slip on the distal faults; (ii) more symmetric slip distributions in the central part of the arrays; (iii) steeper gradients near the fault overlap areas; and (iv) steepest average slip gradients along the central segments. It should be noted that the data points are not spaced closely enough to resolve what happens very close to the fault tips in the relay zones.

The model for three fault segments can be used to understand the concept of *kinematic coherence*: the observation that an array of faults appears to behave similarly to a single fault of the same length as the array (Walsh & Watterson 1991). Consider the fault slip along an originally-horizontal layer that cuts through the centres of the three faults. The slip distribution observed on this layer is shown in Fig. 7(c). The modelled fault segments are kinematically coherent in the sense that the total slip (thick grey curve in Fig. 7c) appears similar to that of one fault with a slightly irregular slip distribution in the central area. The normal fault arrays shown in Fig. 8 exhibit very similar behaviour because the total slip along these arrays is similar to that of single faults, and the irregularities in the slip distribution are associated with the relay zones.

The maximum slip along the central segment (Fig. 7c) can be compared with the maximum slip along a longer continuous fault. For a valid quantitative comparison, the single fault must have the same dimensions as the envelope surrounding the three echelon faults (compare the fault in Fig. 9a with the grey ellipse in Fig. 9b). The maximum slip on the single elliptical fault (1.24) is only slightly greater than the maximum slip across the three echelon faults (1.16). This increase is relatively minor because both models have the same height, stressing the importance of three-dimensional analyses. It appears that a discontinuous overstepping fault geometry does not significantly reduce the capacity to accommodate slip. Figure 10 shows how the maximum slip on the central segment decreases from 1.16 to 1.14 if the fault spacing is increased from $0.05a$ to $0.1a$ and to 1.04 for a fault spacing of $1a$. This change is entirely caused by mechanical interaction which decreases with increased fault spacing. Conversely, as the spacing of the three echelon faults tends to zero, the maximum slip along the

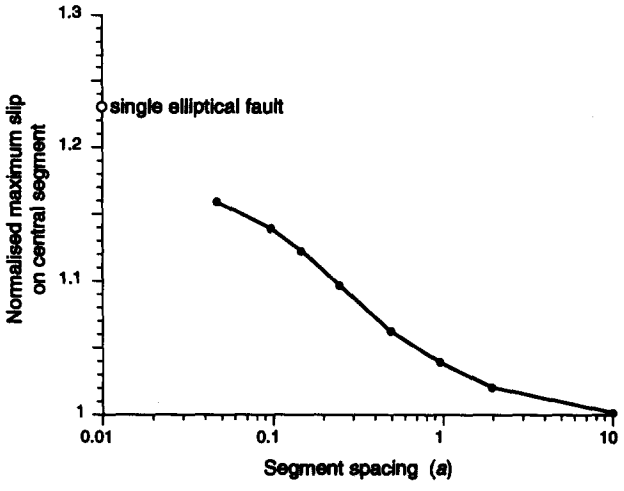

Fig. 10. Example of maximum segment slip as a function of segment spacing. The fault array geometry is shown in Fig. 9(b), with segment overlap of $0.5a$, where a is the fault radius. For large spacings, the maximum slip is nearly identical to that of an isolated circular fault for which the maximum slip is 1. With decreasing segment spacing, the maximum slip increases as the intensity of fault interaction increases. As the spacing tends to zero, the maximum slip tends towards that of the single larger elliptical fault shown in Fig. 9(a).

array tends to that along the single continuous elliptical fault.

The resemblance between a fault array and a single continuous fault is not confined to the slip distribution. The deformation in the wall rock surrounding a fault array is also similar to that about a single elliptical fault that has the same dimensions as the array. The contours of footwall uplift and hangingwall subsidence for the array resemble those surrounding the single elliptical fault (Fig. 9a). The resemblance between wall rock deformation around a single fault and a fault array increases as the spacing between the segments decreases.

CONSEQUENCES FOR SLIP-TO-LENGTH SCALING

A variety of fault scaling laws have been proposed to relate fault slip to fault length. Such relationships are important in earthquake studies (Aki & Richards 1980), for models of fault growth (Watterson 1986, Cowie & Scholz 1992c), and are the basis for predictions of small-scale faulting and fracturing in hydrocarbon and water reservoirs (Gauthier & Lake 1993). For a given fault length, measured slip-to-length ratios appear to vary by about one order of magnitude (Gillespie *et al.* 1992). Because of this variability, and the lack of agreement on how the data should be analysed, the same data have been used to support different growth models (Watterson 1986, Walsh & Watterson 1988, Cowie & Scholz 1992a, Scholz *et al.* 1993). Gillespie *et al.* (1992) comment on sampling problems and stress that the data cannot be analysed satisfactorily by standard statistical methods.

Many recent investigations suggest that faults are scale-invariant, thus proposing a constant slip-to-length ratio (Cowie & Scholz 1992a, Dawers *et al.* 1993, Scholz *et al.* 1993, Anders & Schlische 1994, Dawers & Anders 1995). However, rock anisotropy such as layering can cause departures from self-similarity (Wojtal 1994). Wojtal (1994) and Filbrandt *et al.* (1994) show that scaling constants can change during the temporal evolution of the fault system. The results described in this contribution suggest that variations in slip-to-length ratio should be expected, even for the simplest case of a single slip event in a homogeneous isotropic rock because: (i) faults are not infinite in extent but are bounded in three dimensions; and (ii) because neighbouring faults or fault segments can interact.

The influence of three-dimensional fault shape on the slip distribution has been known since Chinnery (1961) and Scholz (1982). However, the effect of three-dimensional shape on slip magnitude (Fig. 3) has been neglected in the discussion of fault slip-to-length ratios. For a given horizontal fault length, the maximum displacement decreases markedly as the down-dip fault height decreases. For normal faults, the shortest dimension is generally the fault height rather than the horizontal fault length: fault aspect ratios reported for single, isolated normal faults vary between 1 and 4 (Rippon 1985, Barnett *et al.* 1987). Therefore the natural range in three-dimensional fault shape alone leads to variations of at least a factor of 3 in slip-to-length ratios.

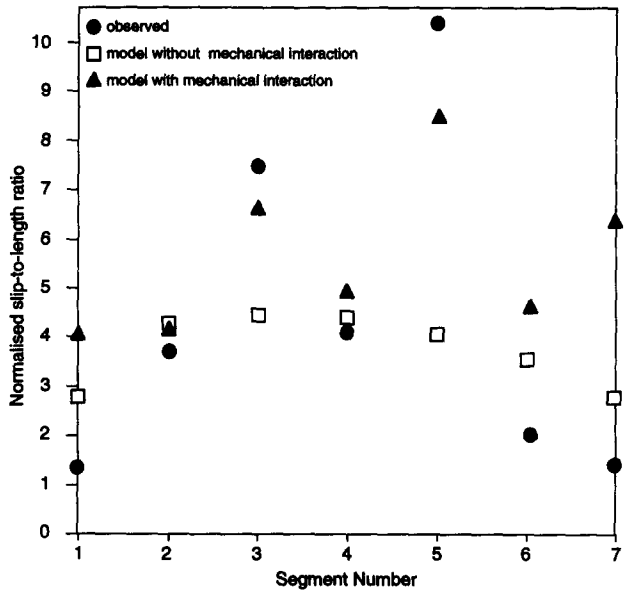

Fig. 11. Fault slip-to-length ratios on fault array in Bishop Tuff from the Volcanic Tableland. The slip distribution is shown in Fig. 8(b). The length-to-slip ratios of individual segments are divided by that of the composite array. Greater ratios occur on the central segments, whereas the ratios on the outer segments are similar to that of the array. The model with mechanical interaction among the segments provides a better fit to the observations than the model without interaction.

Mechanical interaction between fault segments also can influence the slip-to-length ratio. In all the numerical experiments discussed above, mechanical interaction among echelon faults increases the magnitude of the maximum slip. For example, maximum slip magnitudes increase up to about 1.09 for two overlapping fault segments (Fig. 6), and up to 1.16 for the case of three overlapping segments (Fig. 7). A slip magnitude of 1 corresponds to the maximum slip on an isolated fault. Therefore, mechanical interaction increases the slip-to-length ratio.

This effect can become pronounced for fault arrays containing many echelon segments. For example, the slip-to-length ratio on the short middle segment of the array in the Arley Coal Seam (Fig. 8a) is about 1.7 times the ratio for both distal segments and as much as 3 times the ratio of the entire array. The occurrence of greater ratios in the central part of the array, and lesser ratios at the distal ends is consistent with the numerical experiments (Fig. 7c). In the array from the Volcanic Tableland shown in Fig. 8(b), the greatest slip gradients also occur on central segments, and the least slip gradients occur on outer segments. Figure 11 illustrates this quantitatively by showing slip-to-length ratios of the individual segments normalized by the ratio for the entire array. The slip-to-length ratios for the central segments are up to 10 times that of the composite array. The distal segments, however, are characterized by ratios that are comparable to that of the entire array.

Poly3d has been used to investigate whether this variability can be explained by mechanical interaction. A simple model was constructed in which individual segments are represented by a planar half ellipse, with the cut, horizontal side of the ellipse intersecting the surface of the elastic half-space. The segments dip 70° and have the same strike. At the top of the half-space the modelled segment lengths, overlaps and spacings are the same as observed in the outcrop. All segments were assumed to have the same down-dip height and were subjected to a uniform stress drop. In the first experiment, the segments were not allowed to interact mechanically with one another so that the computed slip-to-length ratios are controlled only by differences in three-dimensional segment shape. Figure 11 shows that these computed ratios do not agree well with outcrop observations, especially not for segment number 3 and 5.

In the second experiment, mechanical interaction was allowed. This results in an improved fit to the outcrop data (Fig. 11). In the central part of the array (segments 2–5), there is good correspondence between the measured and computed slip-to-length ratios. Mechanical interaction is thus one possible explanation for the great slip-to-length ratios on the central segments. However, some discrepancy remains at the array ends, where the computed slip is greater than that observed in the field. Possible causes for this discrepancy might include smaller height of the distal segments or increased friction on the distal segments.

CONCLUSIONS

The discontinuous nature of faults in three dimensions has a profound impact on their mechanical behaviour. Our analyses suggest that mechanical interaction between fault segments leads to systematic deviations from simple symmetric slip distributions. Interaction between neighbouring segments can cause off-centre location of maximum slip, asymmetrical slip gradients along underlapping segments, decrease of slip gradients in the relay zones between overlapping segments, and kinematic coherence of fault arrays. The effects of interaction become more pronounced with increasing segment overlap and height, and with decreasing spacing.

These relationships between three-dimensional fault geometry, spatial fault arrangement and slip distribution can be applied to practical problems in various ways. For example, the magnitude of the maximum slip along an outcropping isolated normal fault might be used to estimate the fault height: larger slip magnitudes suggest taller faults. For two interacting normal faults, the degree of asymmetry in the slip distribution can provide another indication on the fault height: shorter faults interact less and exhibit more symmetric slip distributions than taller faults. We have also shown that individual segments in a fault array have a tendency to grow until some degree of overlap with the neighbouring segments is obtained.

The results indicate that field data need to be analysed very carefully in their geometrical context, taking into account both the three-dimensional fault shape and the influence of potential neighbouring structures. An example is the analysis of fault slip-to-length ratios. The slip-to-length ratio for isolated normal faults can vary by a factor of about 3 for the range of fault shapes observed. The slip-to-length ratio within fault arrays can vary by an order of magnitude because of mechanical interaction. Fault scaling laws based on two-dimensional models of single, continuous faults are incapable of capturing this variability. The numerical experiments predict a range of more than an order of magnitude in slip-to-length ratio for the simple case of a single slip event along faults in a rock mass with homogeneous isotropic linear elastic material properties and uniform loading conditions. The greater variation observed in field data (Gillespie *et al.* 1992) is to be expected because of the more complex conditions found in nature.

Our fault model captures some of the mechanics of an idealized single slip event. The results obtained correspond well with the slip distributions along some earthquake ruptures and ancient normal faults. The correspondence with the slip along the ancient faults is remarkable because their final slip distribution is affected by many factors that have not been considered here such as size of the slip patch, temporal changes in the stress field, spatial variations in material properties, effects of fault growth, development of permanent strains in the host rock material, inelastic deformation near the fault tips, etc. (Bürgmann *et al.* 1994, Peacock & Sanderson 1996). Although the role of these parameters needs to be analysed further as the appropriate fault models become available, the good correspondence between our model and the field data is encouraging. Apparently some first-order complexities in natural slip distributions can be understood using relatively simple mechanical models.

Acknowledgements—Financial support by the Rock Fracture Project at Stanford University, by a Shell Research B.V. (The Netherlands) summer grant, and by a Phillips Petroleum Co. fellowship to E. Willemse are gratefully acknowledged. A McGee grant from the Department of Geological and Environmental Sciences partly covered field-work expenses. David Peacock and Rob Knipe provided very helpful and thorough reviews. Many thanks to Marco Antonellini for assistance in the field, David Peacock and Roland Bürgmann for stimulating discussions, Nancye Dawers for sending an early version of her manuscript, and to Fer, Marie-Thérèse and Paula for support.

REFERENCES

Aki, K. 1979. Characterization of barriers on an earthquake fault. *J. geophys. Res.* **84**, 6140–6148.

Aki, K. 1989. Geometric features of a fault zone related to the nucleation and termination of an earthquake rupture. In: *Fault Segmentation and Controls of Rupture Initiation and Termination* (edited by Schwartz, D. P. & Sibson, R. H.). *U.S. geol. Surv. Open-file Rep.* **89–315**, 1–9.

Aki, K. & Richards, P. G. 1980. *Quantitative Seismology Theory and Methods*. W. H. Freeman, San Francisco.

Anders, M. H. & Schlische, R. W. 1994. Overlapping faults, intrabasin highs, and the growth of normal faults. *J. Geol.* **102**, 165–180.

Aydin, A. & Nur, A. 1982. Evolution of pull-apart basins and their scale independence. *Tectonics* **1**, 91–105.

Aydin, A. & Nur, A. 1985. The types and role of stepovers in strike-slip tectonics. In: *Strike-slip Deformation, Basin Formation and Sedimentation* (edited by Biddle, K. T. & Christie-Blick, N.). *Spec. Publ. Soc. econ. Paleontol. Miner.* **37**, 35–45.

Aydin, A. & Schultz, R. A. 1990. Effect of mechanical interaction on the development of strike-slip faults with echelon patterns. *J. Struct. Geol.* **12**, 123–129.

Bakun, W. H., King, G. C. P. & Cockerham, R. S. 1986. Seismic slip, aseismic slip, and the mechanics of repeating earthquakes on the Calaveras Fault, California. In: *Earthquake Source Mechanics* (edited by Das, S., Boatwright, J. & Scholz, C. H.). *Am. Geophys. Un. Geophys. Monogr., Maurice Ewing Series* **6**, 195–206.

Bakun, W. H., Stewart, R. M., Bufe, C. G. & Marks, S. M. 1980. Implications of seismicity for failure of a section of the San Andreas Fault. *Bull. seism. Soc. Am.* **79**, 185–201.

Barka, A. A. & Kadinshy-Cade, K. 1988. Strike-slip fault geometry in Turkey, and influence on earthquake activity. *Tectonics* **7**, 663–684.

Barnett, J. M., Mortimer, J., Rippon, J., Walsh, J. J. & Watterson, J. 1987. Displacement geometry in the volume containing a single normal fault. *Bull. Am. Ass. Petrol. Geol.* **71**, 925–937.

Barr, D. 1985. 3-D palinspastic restoration of normal faults in the Inner Moray Firth: implications for extensional basin development. *Earth & Planet. Sci. Lett.* **75**, 191–203.

Bateman, P. C. 1965. Geology and Tungsten mineralisation of the Bishop District, California. *Prof. Pap. U.S. geol. Surv.* **470**, 1–208.

Becker, A. A. 1992. *The Boundary Element Method in Engineering*. McGraw-Hill, New York.

Bouvier, J. D., Kaars-Sijpesteijn, C. H., Kluesner, D. F., Onyejekwe, C. C. & Van Der Pal, R. C. 1989. Three-dimensional seismic interpretation and fault sealing investigations, Nun River Field, Nigeria. *Bull. Am. Ass. Petrol. Geol.* **73**, 1397–1414.

Bürgmann, R., Pollard, D. D. & Martel, S. J. 1994. Slip distributions on faults: effects of stress gradients, inelastic deformation, heterogeneous host-rock stiffness, and fault interaction. *J. Struct. Geol.* **16**, 1675–1690.

Childs, C., Easton, S. J., Vendeville, B. C., Jackson, M. P. A., Lin, S. T., Walsh, J. J. & Watterson, J. 1993. Kinematic analysis of faults in a physical model of growth faulting above a viscous salt analogue. *Tectonophysics* **228**, 313–329.

Childs, D., Watterson, J. & Walsh, J. J. 1995. Fault overlap zones within developing normal fault systems. *J. geol. Soc. Lond.* **152**, 535–549.

Chinnery, M. A. 1961. The deformation of the ground around surface faults. *Bull. seism. Soc. Am.* **51**, 355–372.

Cloos, E. 1955. Experimental analysis of fracture patterns. *Bull. geol. Soc. Am.* **66**, 241–256.

Cloos, H. 1928. Experimente zur inneren Tektonik. *Ctbl. Mineral. Geol. Palaeont.* **1928B**, 609–621.

Comninou, M. A. & Dunders, J. 1975. The angular dislocation in a half-space. *J. Elastic.* **5**, 203–216.

Cowie, P. A. & Scholz, C. H. 1992a. Displacement–length relationship for faults: data synthesis and discussion. *J. Struct. Geol.* **14**, 1149–1156.

Cowie, P. A. & Scholz, C. H. 1992b. Growth of faults by accumulation of seismic slip. *J. geophys. Res.* **97**, 11,085–11,095.

Cowie, P. A. & Scholz, C. H. 1992c. Physical explanation for the displacement–length relationship of faults, using a post-yield fracture mechanics model. *J. Struct. Geol.* **14**, 1133–1148.

Crouch, S. L. & Starfield, A. M. 1983. *Boundary Element Methods in Solid Mechanics*. George Allen & Unwin, London.

Davy, P. 1993. On the frequency–length distribution of the San Andreas Fault system. *J. geophys. Res.* **98**, 12,141–12,151.

Dawers, N. H. & Anders, M. H. 1995. Displacement–length scaling and fault linkage. *J. Struct. Geol.* **17**, 607–614.

Dawers, N. H., Anders, M. H. & Scholz, C. H. 1993. Growth of normal faults: displacement–length scaling. *Geology* **21**, 1107–1110.

Delaney, P. T. & Pollard, D. D. 1981. Deformation of host rocks and flow of magma during growth of minette dikes and breccia-bearing intrusions near Ship Rock, New Mexico. *Prof. Pap. U.S. geol. Surv.* **1202**, 1–61.

Deng, Q., Shefa, C., Fangmin, S., Shilong, Z., Yipeng, W., Weiqi, Z., Decheng, J., Burchfield, B. C., Molnar, P., Royden, L. & Peizhen, Z. 1986. Variations in the geometry and amount of slip on the Haiyuan (Nanxihaushan) fault zone, China, and the surface rupture of the 1920 Haiyuan earthquake. In: *Earthquake Source Mechanics* (edited by Das, S., Boatwright, J. & Scholz, C. H.). *Am. Geophys. Un. Geophys. Monogr., Maurice Ewing Series* **6**, 169–182.

Deng, Q. & Zhang, P. 1984. Research on the geometry of shear fracture zones. *J. geophys. Res.* **89**, 5699–5710.

Ellis, M. A. & Dunlap, W. J. 1988. Displacement variation along thrust faults: implications for the development of large faults. *J. Struct. Geol.* **10**, 183–192.

Eshelby, J. D. 1957. The determination of the elastic field of an ellipsoidal inclusion and related problems. *Proc. R. Soc. Lond.* **A241**, 376–396.

Filbrandt, J. M., Richard, P. D. & Franssen, R. C. M. W. 1994. Growth and coalescence of faults: numerical simulations and sandbox experiments. In: *TSG Special Meeting on Fault Populations*, Edinburgh, U.K., Extended Abstracts, 57–59.

Gamond, J. F. 1983. Displacement features associated with fault zones: a comparison between observed examples and experimental models. *J. Struct. Geol.* **5**, 33–45.

Gauthier, B. D. M. & Lake, S. D. 1993. Probabilistic modeling of faults below the limit of seismic resolution in Pelican Field, North Sea, offshore United Kingdom. *Bull. Am. Ass. Petrol. Geol.* **77**, 761–777.

Gay, N. C. & Ortlepp, W. D. 1979. Anatomy of a mining-induced fault zone. *Bull. geol. Soc. Am.* **90**, 47–58.

Gibbs, A. D. 1990. Linked fault families in basin formation. *J. Struct. Geol.* **12**, 795–803.

Gillespie, P. A., Walsh, J. J. & Watterson, J. 1992. Limitations of dimension and displacement data from single faults and the consequences for data analysis and interpretation. *J. Struct. Geol.* **14**, 1157–1172.

Goguel, J. 1950. *Traite de Tectonique*, 1st edn. Masson, Paris.

Jev, B. I., Kaars-Sijpesteijn, C. H., Peters, M. P. A. M., Watts, N. L. & Wilkie, J. T. 1993. Akaso Field, Nigeria: Use of integrated 3-D seismic, fault slicing, clay smearing, and RFT–pressure data on fault trapping and dynamic leakage. *Bull. Am. Ass. Petrol. Geol.* **77**, 1389–1404.

Jeyakumaran, M., Rudnicki, J. W. & Kerr, L. M. 1992. Modeling slip zones with triangular dislocation elements. *Bull. seism. Soc. Am.* **82**, 2153–2169.

King, G. C. P. 1986. Speculations on the geometry of the initiation and termination process of earthquake rupture and its relation to morphology and geological structure. *Pure & Appl. Geophys.* **124**, 567–585.

King, G. C. P., Lindh, A. G. & Oppenheimer, D. 1990. Seismic slip, segmentation and the Loma Prieta earthquake. *Geophys. Res. Lett.* **7**, 1445–1452.

King, G. C. P. & Nabelek, J. 1985. Role of fault bends in the initiation and termination of earthquake rupture. *Science* **228**, 984–987.

Kronberg, P. 1991. Geometries of extensional fault systems, observed and mapped on aerial and satellite photographs of Central Afar, (Ethiopia/Djibouti). *Geologie Mijnb.* **70**, 145–161.

Larsen, P. H. 1988. Relay structures in a Lower Permian basement-involved extension system, East Greenland. *J. Struct. Geol.* **10**, 3–8.

Lawson, A. C. & others. 1908. The California Earthquake of April 18, 1906. In: *Report of the State Earthquake Investigation Commission*. Carnegie Institute of Washington, Washington, DC, 641.

Ma, X. Q. & Kusznir, N. J. 1993. Modelling of near-field subsurface displacements for generalized faults and fault arrays. *J. Struct. Geol.* **15**, 1471–1484.

Mandl, G. 1987a. Discontinuous fault zones. *J. Struct. Geol.* **9**, 105–110.

Mandl, G. 1987b. Tectonic deformation by rotating parallel faults: the "bookshelf" mechanism. *Tectonophysics* **141**, 277–316.

Mandl, G. 1988. *Mechanics of Tectonic Faulting: Models and Basic Concepts*. Elsevier, Amsterdam.

Marrett, R. & Allmendinger, R. W. 1991. Estimates of strain due to brittle faulting: sampling of fault populations. *J. Struct. Geol.* **13**, 735–738.

Martel, S. J. & Pollard, D. D. 1989. Mechanics of slip and fracture along small faults and simple strike-slip fault zones in granitic rock. *J. geophys. Res.* **94**, 9417–9428.

Martel, S. J., Pollard, D. D. & Segall, P. 1988. Development of simple strike-slip fault zones, Mount Abbot quadrangle, Sierra Nevada, California. *Bull. geol. Soc. Am.* **100**, 1451–1465.

Moore, J. M. 1979. Tectonics of the Najd transcurrent fault system, Saudi Arabia. *J. geol. Soc. Lond.* **136**, 441–452.

Morley, C. K., Nelson, R. A., Patton, T. L. & Munn, S. G. 1990. Transfer zones in the East African rift system and their relevance to hydrocarbon exploration in rifts. *Bull. Am. Ass. Petrol. Geol.* **74**, 1234–1253.

Muraoka, H. & Kamata, H. 1983. Displacement distribution along minor fault traces. *J. Struct. Geol.* **5**, 483–495.

Naylor, M. A., Mandl, G. & Kaars-Sijpesteijn, C. H. 1986. Fault geometries in basement-induced wrench faulting under different initial stress states. *J. Struct. Geol.* **8**, 737–752.

Palmer, A. C. & Rice, J. R. 1973. The growth of slip surfaces in the progressive failure of overconsolidated clay. *Proc. R. Soc. Lond.* **A332**, 527–548.

Peacock, D. C. P. 1991. Displacement and segment linkage in strike-slip fault zones. *J. Struct. Geol.* **13**, 1025–1035.

Peacock, D. C. P. & Sanderson, D. J. 1991. Displacements, segment linkage and relay ramps in normal fault zones. *J. Struct. Geol.* **13**, 721–733.

Peacock, D. C. P. & Sanderson, D. J. 1994. Geometry and development of relay ramps in normal fault systems. *Bull. Am. Ass. Petrol. Geol.* **78**, 147–165.

Peacock, D. C. P. & Sanderson, D. J. 1996. Effects of propagation rate on displacement variations along faults. *J. Struct. Geol.* **18**, 311–320.

Pollard, D. D. & Segall, P. 1987. Theoretical displacements and stresses near fractures in rock: with applications to faults, joints, veins, dikes, and solution surfaces. In: *Fracture Mechanics of Rocks* (edited by Atkinson, B. K.). *Academic Press Geology Series*. Academic Press, London.

Raynaud, S. 1987. Les premiers stades de la deformation dans une zone de relais entre decrochements: exemples naturels et experimentaux. *Bull. Soc. geol. Fr.* **8**, 583–590.

Rice, J. R. 1979. Theory of precursory processes in the inception of earthquake rupture. *Gerlands Beitr. Geophys.* **88**, 91–127.

Rice, J. R. & Rudnicki, J. W. 1979. Earthquake precursory effects due to pore fluid stabilization of a weakening fault zone. *J. geophys. Res.* **84**, 2177–2193.

Riedel, W. 1929. Zur Mechanik geologischer Brucherscheinungen. *Ctbl. Mineral. Geol. Palaeont.* **1929B**, 354–368.

Rippon, J. H. 1985. Contoured patterns of throw and hade of normal faults in the coal measures (Westphalian) of northeast Derbyshire. *Proc. Yorks. geol. Soc.* **45**, 147–161.

Rudnicki, J. W. 1977. The inception of faulting in a rock mass with a weakened zone. *J. geophys. Res.* **82**, 844–854.

Rudnicki, J. W. 1979. Rotation of principal stress axes caused by faulting. *Geophys. Res. Lett.* **6**, 135–138.

Rymer, M. J. 1989. Surface rupture in a fault stepover on the Superstition Hills fault, California. In: *Fault Segmentation and Controls of Rupture Initiation and Termination* (edited by Schwartz, D. P. & Sibson, R. H.). *U.S. geol. Surv. Open-file Rep.* **89–315**, 309–323.

Scholz, C. H. 1982. Scaling laws for large earthquakes: consequences for physical models. *Bull. seism. Soc. Am.* **72**, 1–14.

Scholz, C. H., Dawers, N. H., Yu, J. Z. & Anders, M. H. 1993. Fault growth and fault scaling laws: preliminary results. *J. geophys. Res.* **98**, 21,951–21,961.

Schwartz, D. P. & Coppersmith, K. J. 1984. Fault behavior and characteristic earthquakes: examples from the Wasatch and San Andreas Fault zones. *J. geophys. Res.* **89**, 5681–5698.

Segall, P. & Pollard, D. D. 1980. Mechanics of discontinuous faults. *J. geophys. Res.* **85**, 4337–4350.

Sherridan, M. F. 1975. Tectonic displacement in the Bishop Tuff. *Calif. Geol.* **28**, 107–108.

Sibson, R. H. 1986. Rupture interaction with fault jogs. In: *Earthquake Source Mechanics* (edited by Das, S., Boatwright, J. & Scholz, C. H.). *Am. Geophys. Un. Geophys. Monogr., Maurice Ewing Series* **6**, 157–167.

Sibson, R. H. 1987. Effects of fault heterogeneity on rupture propagation. In: *Directions in Paleoseismology* (edited by Crone, A. J. & Omdahl, E. M.). *U.S. geol. Surv. Open-file Rep.* **87–673**, 362–373.

Sibson, R. H. 1989. Earthquake faulting as a structural process. *J. Struct. Geol.* **11**, 1–14.

Sieh, K. 1978. Slip along the San Andreas fault associated with the great 1857 earthquake. *Bull. seism. Soc. Am.* **68**, 1421–1428.

Sieh, K. E. 1981. A review of geological evidence for recurrence times of large earthquakes. In: *Earthquake Prediction: An International Review* (edited by Simpson, D. & Richards). *Am. Geophys. Un. Geophys. Monogr., Maurice Ewing Series* **4**, 181–207.

Sih, G. C. 1975. *Three Dimensional Crack Problems*. Noordhoff International, Leiden.

Tada, H., Paris, P. C. & Irwin, G. R. 1985. *The Stress Analysis of Cracks Handbook*. Paris Productions Incorporated (& Del Research Corporation), St. Louis.

Tchalenko, J. S. 1970. Similarities between shear zones of different magnitudes. *Bull. geol. Soc. Am.* **81**, 1625–1640.

Tchalenko, J. S. & Ambraseys, N. N. 1970. Structural analysis of Dasht-e Bayaz (Iran) earthquake fractures. *Bull. geol. Soc. Am.* **81**, 41–60.

Tchalenko, J. S. & Berberian, M. 1975. Dasht-e Bayaz Fault, Iran: Earthquake and Earlier related structures in bed rock. *Bull. geol. Soc. Am.* **86**, 703–709.

Thatcher, W. & Bonilla, M. 1989. Earthquake fault slip estimation from geologic, geodetic and seismologic observations: implications for earthquake mechanics and fault segmentation. In: *Fault Segmentation and Controls of Rupture Initiation and Termination* (edited by Schwartz, D. P. & Sibson, R. H.). *U.S. geol. Surv. Open-file Rep.* **89–315**, 386–399.

Thomas, A. L. 1993. Poly3D : a three-dimensional, polygonal element, displacement discontinuity boundary element computer program with applications to fractures, faults, and cavities in the Earth's crust. M.Sc. thesis, Stanford University, California.

Wallace, R. E. 1973. Source fracture patterns along the San Andreas fault. In: *Conference on Tectonic Processes of the San Andreas Fault System, Vol. XIII* (edited by Kovach, R. L. & Nur, A.). Stanford University Press, 248–250.

Walsh, J. J. & Watterson, J. 1987. Distributions of cumulative displacement and seismic slip on a single normal fault surface. *J. Struct. Geol.* **9**, 1039–1046.

Walsh, J. J. & Watterson, J. 1988. Analysis of the relationship between displacements and dimensions of faults. *J. Struct. Geol.* **10**, 239–247.

Walsh, J. J. & Watterson, J. 1990. New methods of fault projection for coalmine planning. *Proc. Yorks. geol. Soc.* **48**, 209–219.

Walsh, J. J. & Watterson, J. 1991. Geometric and kinematic coherence and scale effects in normal fault systems. In: *The Geometry of Normal Faults* (edited by Roberts, A. M., Yielding, G. & Freeman, B.). *Spec. Publs geol. Soc. Lond.* **56**, 193–203.

Watterson, J. 1986. Fault dimensions, displacements and growth. *Pure & Appl. Geophys.* **124**, 365–373.

Wojtal, S. F. 1994. Fault scaling laws and temporal evolution of fault systems. *J. Struct. Geol.* **16**, 603–612.

Yeats, R. S. & Schwartz, D. P. 1990. Paleoseismicity: extending the record of earthquakes into pre-historic time. *Episodes* **13**, 9–12.

Zhang, P., Slemmons, D. B. & Mao, F. 1991. Geometric patterns, rupture termination and fault segmentation of the Dixie Valley–Pleasant Valley active normal fault system, Nevada, U.S.A. *J. Struct. Geol.* **13**, 165–176.